 doi:10.20944/preprints201807.0006.v1

Article

Microparticle Inertial Focusing in an Asymmetric Curved Microchannel

Arzu Özbey [1], Mehrdad Karimzadehkhouei [2], Hossein Alijani [3] and Ali Koşar [1,2,3,*]

[1] Faculty of Engineering and Natural Science, Mechatronics Engineering Program, Sabanci University, Tuzla, Istanbul 34956, Turkey; ozbeyarzu@sabanciuniv.edu (A.O.); mehrdad@sabanciuniv.edu (M.K.); hossein@sabanciuniv.edu (H.A.)
[2] Center of Excellence for Functional Surfaces and Interfaces for Nano-Diagnostics (EFSUN), Sabanci University, Tuzla, Istanbul 34956, Turkey
[3] Sabanci University, SUNUM Nanotechnology Research Center, Tuzla, Istanbul 34956, Turkey
* Correspondence: kosara@sabanciuniv.edu; Tel.: +90-216-483-9621

Abstract: Inertial microfluidics offers high throughput, label-free, easy to design, and cost-effective solutions and is a promising technique based on hydrodynamic forces (passive techniques) instead of external ones, which can be employed in lab-on-a-chip and micro-total-analysis-systems for focusing, manipulation, and separation of microparticles in chemical and biomedical applications. The current work, studies the focusing behavior of microparticles in an asymmetric curvilinear microchannel. For this purpose, focusing behavior, including position and band width, of microparticles of diameters of 10, 15 and 20 μm, which served as representatives of different cells, in an asymmetric curvilinear microchannel with curvature angle of 280° was experimentally studied at flow rates from 400 to 2700 μL/min (corresponding to Reynolds numbers between 30 and 205). The results revealed that the largest distance between focusing bands of 20 μm and 10 μm microparticles as well as between focusing bands of 15 μm and 10 μm was obtained at Reynolds number of 121. For the case of microparticles of diameters 20 μm and 15 μm, the largest distance was seen at Reynolds number of 144. The focusing band width became smaller in the asymmetric microchannel so that focusing could be more clearly observed in this configuration.

Keywords: microfluidics; inertial focusing; fluorescent particle focusing; curvilinear microchannel

1. Introduction

The rapid advances in Microfluidics and Nanofluidics fields have made compact microfluidic devices and emerging cell applications to offer potential benefits in providing lab-on-a-chip (LOC) platforms for disease diagnosis and treatment [1–7]. Thanks to major progresses in micro/nano fabrication techniques, microfluidic applications in various subjects, such as DNA analysis [1–3], cytometry [4,5], micromixing [6] and microreactors [7] have appeared over the past decades. One of the distinct advantages of microfluidic systems is their capability to be integrated into other systems. In particular, the use of LOC platforms allowed the combination of several methods within a single device [8]. For instance, the micro-total-analysis systems (μTAS) were designed by combining different applications/components such as cytometers, bioreactors and separation into a single system [9]. Such an integrated system covering a small area requires very low amounts of fluids during its operation [8,10–13].

Particle separation and detection of some cells or biomolecules are one of the most studied topics in this area. Active or passive methods are the major categories of separation techniques [14,15]. While the former utilizes an external force [16,17] such as magnetic [18], dielectric [19] or acoustic [20], the latter relies on channel geometry and internal forces only. Passive separation methods mainly exploit

 doi:10.20944/preprints201807.0006.v1

hydrodynamic forces in microscale and heavily depend on surface properties of the microchannel geometry. Furthermore, since fabricating passive separation devices is less complicated than active ones, integrating them into a lab-on-a-chip device is also much simpler. Moreover, the ability of designing parallel microchannels could provide a higher throughput in such a device.

Typically, microchannels can be classified as straight [21–29], straight with contraction and expansion regions [30–36] and curvilinear channels including spiral [37–44] and serpentine [45–48] channels. Depending upon the balance of hydrodynamic forces acting on microparticles or cells, they pass along specific paths in the flow direction, known as focusing (focal, or equilibrium) position. The present forces are functions of the microchannel geometry, fluid properties and microparticles dimensions and shape. In straight channels, Reynolds number and the cross section of the microchannel are the two major parameters that determine the focal position of the microparticles. As an instance, the microparticles that flow at moderate Reynolds numbers inside an straight microchannel with square cross section, focus at four equilibrium locations at the center of the walls; while in low aspect ratio rectangular cross sections, the microparticles focus along the center of the two long edges [27].

Curved geometries induces secondary flows especially in regions with fading lateral force. Therefore, introducing curvilinearity to a microchannel with rectangular cross section yields in better controlling the number and position of equilibrium positions; in better words, handling the focal positions is eased in curved microchannels [49–51]. In curvilinear microchannels, the velocity of the fluid passing along the centerline differs from that of the fluid that passes near the walls. Consequently, the inertia is increased near the centerline. Thus, a pressure gradient in the radial direction is generated and the fluids near the inner and outer walls tends to switch their positions by moving in transversal directions of outward and inward, respectively. Therefore, two symmetric vortices, which introduce Dean drag force (DDF) to the system, form [49,51]. Spiral [44] and curved serpentine [52] microchannels are the two main categories of curvilinearity. Particularly, designs of curvilinear serpentine channels include symmetric [52,53] and asymmetric [46,54,55] geometries. Extensive experiments on microparticle focusing in straight and symmetric and asymmetric curved serpentine channels were carried out by Di Carlo et al [52].

In this study, focusing behavior of polystyrene microparticles in an asymmetric curvilinear microchannel with curvature angle of 280° was experimentally studied. In this regard, particles of 10, 15 and 20 μm diameter were pumped into the microchannel with flow rates between 400 and 2700 μL/min, equivalent to Reynolds numbers range of 30-205. At each Reynolds number, focusing position of each particle along with the focusing width was measured and reported in two particular regions: the transition region, which is the inflection point of the last two curves, and the outlet region. Moreover, for each binary combination of the particles, the optimum Reynolds number, defined as the one at which the largest distance between the focal bands of two particles at the transition region occurs, was reported. Lastly, the focusing behavior of the particles in the current asymmetric microchannel was compared to the symmetric design with the same curvature angle, previously done in our group [53].

2. Theoretical Background

Understanding the forces acting on microparticles or cells plays an important role in accurately predicting their focal positions. The main forces applying on microparticles in microchannels include shear gradient lift force (SGLF) and wall induced lift force (WILF). In curved microchannels, additionally, there exists a DDF due to the formation of secondary flow. It should be mentioned that all of these forces are in transverse direction (Figure 1).

For a microparticle in fluid flow, because of the parabolic velocity profile of the Poiseuille flow, its upper side has a larger relative velocity (in magnitude) than its lower side. This reduces the pressure on the upper side of the particle and, consequently, a SGLF is generated, by which the particle is pushed away from the centerline towards the channel walls until this force is balanced by WILF [56,57]. In other words, a particle tends to follow the path along which its sides undergo minimum difference in relative velocity. The magnitude of the SGLF is given as:

Preprints (www.preprints.org) | NOT PEER-REVIEWED | Posted: 2 July 2018 doi:10.20944/preprints201807.0006.v1

$$F_S = C_L \frac{\rho U_{max}^2 a^3}{D_h} \quad (1)$$

where C_L is the lift coefficient, ρ is the fluid density, U_{max} is the maximum velocity of the fluid, a is the diameter of the microparticle, and D_h is the channel hydraulic diameter. Accordingly, SGLF is strongly affected by the position and diameter of the particle and fluid velocity, while it is independent of particle rotation [58,59].

In addition, there are two main reasons that the particles experience the WILF [60,61]. When a particle moves near a wall of the channel, the wall breaks the axisymmetry of the wake vorticity distribution, which is generated at the particle's surface. As a result, an induced velocity emerges, further breaks the symmetry and generates a WILF that repels the particle. Moreover, the presence of the walls makes the particle to move with a velocity somewhat smaller than that of the fluid [50,58]. Secondly, because of the particle-flow interaction, flow streamlines are deviated towards the particle's sides, and the relative fluid velocity is accelerated on the upper part of the particle, thereby creating low pressure on this side. Therefore, the particle is repelled away from the wall by a WILF. It is worth mentioning that the magnitude of this force increases as the distance between the particle and the wall decreases. WILF is expressed as:

$$F_W = C_W \frac{\rho U_{max}^2 a^6}{D_h^4} \quad (2)$$

where C_W is the lift coefficient, which depends on the position of the particle in the channel and the Reynolds number of the fluid [58,59]. Notably, the two aforementioned lift forces have opposite directions when applying on a microparticle.

Moreover, the net inertial lift force (NILF), F_L, is calculated by the formula:

$$F_L = C_L \frac{4\rho U_f^2 a^4}{D_h^2} \quad (3)$$

where U_f is the mean flow velocity. The lift coefficient, C_L, depends on the channel Reynolds number, Re_c, and the location of the particle in the channel. For the case of Re_c lower than one hundred, C_L is approximated as 0.5 [40,62]. In addition, the NILF has an inverse relationship with Reynolds number [51].

When SGLF and WILF are in balance, according to the tubular pinch effect, particles may focus along an equilibrium position. Successful focusing of the particles occurs when the magnitude of particle diameter over channel hydraulic diameter, $\lambda = a/D_h$, is greater than 0.07 for $Re_p > 1$ [52], where Re_p, particle Reynolds number, is calculated by the formula:

$$Re_p = Re_c \left(\frac{a}{D_h}\right)^2 \quad (4)$$

Particles' focusing positions can be further controlled by using curved geometries [49,51]. As mentioned previously, in curved microchannels the inertia force is higher in magnitude in the centerline. On one hand, the fluid passing along the centerline generates a pressure gradient by flowing outwards. The resultant centrifugal pressure gradient, on the other hand, makes the fluid in the proximity of the outer wall to flow inwards. This results in the formation of two symmetric vortices in a curved microchannel, the so-called secondary flow that exerts DDF, F_D, on the particle, the magnitude of which is calculated through the formula [43]:

$$F_D = 3\pi\mu U_{De} a \quad (5)$$

where the viscosity of the fluid is denoted as μ and U_{De} is the average Dean velocity defined as:

$$U_{De} = 1.8 \times 10^{-4} De^{1.63} \quad (6)$$

In this formula, De is the dimensionless Dean number, given as:

$$De = \frac{\rho U_f D_h}{\mu} \sqrt{\frac{D_h}{2R}} = Re_c \sqrt{\frac{D_h}{2R}} \quad (7)$$

where R is channel curvature radius [51].

Overall, in curved microchannels, the particles focus in a location at which all of the above-mentioned forces constitute an equilibrium.

Preprints (www.preprints.org) | NOT PEER-REVIEWED | Posted: 2 July 2018 doi:10.20944/preprints201807.0006.v1

3. Materials and Methods

2.1 Microchannel Fabrication

The microchannel was made of polydimethylsiloxane (PDMS) through the standard soft lithography fabrication techniques. The steps below were followed to fabricate the chip: a) spinning SU-8 3050 photoresist (Microchem Corp.) on the polished side of a 3'' silicon wafer using a spinner (Dorutek), b) soft baking the photoresist layer, followed by UV exposure of the photoresist with a Mask Aligner UV-Lithography device (Midas System Co., Ltd., MDA-60MS Mask Aligner) through an image reversal acetate mask containing printed geometry of the microchannel printed with 10000 DPI resolution (by CAD/Art Services, Inc.), c) after hard bake, developing unexposed parts of the photoresist by SU-8 Developer (Microchem Corp.), d) pouring a well-mixed mixture of 10 to 1 (weight to weight) ratio of PDMS prepolymer (Sylgard 184, Dow Corning) to curing agent (Sylgard 184 silicone elastomer kit, Dow Corning) over the silicon master contained in a glass petri dish, e) one-hour degassing of PDMS in a vacuum oven (Sheldon Manufacturing, Inc.) under low pressure (76 mmTorr) to eliminate the trapped air bubbles followed by curing for 12 hours at 75°C, f) peeling off the PDMS from the silicon master and cutting it using a bladed instrument, g) punching holes for inlet and outlets by a 21-gauge needle, h) subsequent to cleaning both pieces with Isopropyl alcohol (IPA) and deionized (DI) water and drying by Nitrogen blow, bonding the PDMS to a microscopic glass slide by an oxygen plasma bonding device (Harrick Plasma Cleaner) activating for 60 s, i) resting the PDMS chip on a hotplate (Dorutek) at 75°C for 15 minutes to make the bond stronger.

2.2 Particle Suspensions

Neutrally buoyant fluorescent polystyrene microparticles having diameters of 20 μm (Phosphorex), 15 μm (Invitrogen) and 10 μm (Invitrogen) were employed in the focusing experiments. In this context, they are called 'small,' medium' and 'large' particles, respectively. To decrease particle-particle interaction, low particle concentration was used. For this purpose, weight fraction of the microparticles was fixed at 0.01%, and the solution was diluted, with an initial 1% weight concentration, with DI-water.

2.3 Experimentation

The suspension of each particle was loaded to a 50 mL plastic syringe and pumped into the microchannel by a syringe pump (Harvard Apparatus PHD 2000) with flow rates varying from 400 μL/min to 2700 μL/min with 100 μL/min increments. Each test corresponding to a flow rate lasted for 90 seconds. TYGON tubing (IDEX Corp., IL, internal diameter: 250 μm, length: 150 mm) and appropriate fittings (IDEX Corp., IL) were used for connecting the tip of the syringe to the inlet of the chip and the outlet of the chip to the outlet reservoir. Each experiment was performed three times and the results were consistent in all the three times.

2.4 Fluorescent imaging and data analysis

An inverted phase contrast microscope (Olympus IX72) having a (12-bit) charge coupled camera (Olympus DP 72) and mercury lamp (Olympus U-LH100HG) with 600 ms exposure time was used to take videos of the particles flow. Video processing was done in the Olympus (Olympus VS120-S5), ImageJ and OriginPro-2015 software as follows: a) composite stacking of discrete frames, b) plotting the line profiles along the desired cross section of the microchannel to measure the length of migration and width of the focal band, c) achieving representative pixel columns in the Reynolds number maps, d) exporting Reynolds number maps by applying intensity graphs at different flow rates for individual frames on X-X' and Y-Y' cross sections for the transition and outlet regions (Figure 1(a)), respectively, e) obtaining counter graphs leading to pixel maps.

Preprints (www.preprints.org) | NOT PEER-REVIEWED | Posted: 2 July 2018 doi:10.20944/preprints201807.0006.v1

4. Results and Discussion

The geometry of the asymmetric curvilinear microchannel is depicted in Figure 1(a). It is a repeated pattern of two different curves: 1) 280-degree curves of uniform width of 350 μm followed by 2) 280-degree curves with varying width from 350 μm to 500 μm. There are 11 inflection points in total. The height of the microchannel is 90 μm. Although originally two inlets were considered for the microchannel, in current work the particles flow through one inlet only. Moreover, the Reynolds numbers reported in this study were calculated at the beginning of the inlet, where the microchannel has uniform width of 350 μm.

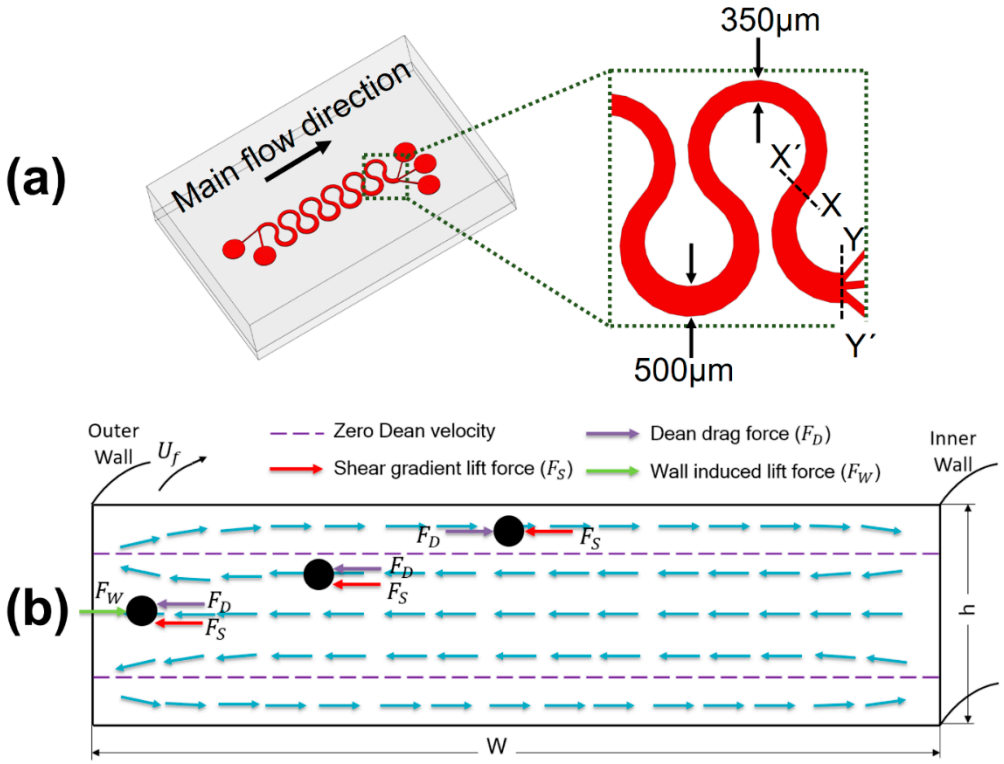

Figure 1. (**a**) Drawing of the asymmetric microchannel and a zoomed-in view of the transition region (X-X') and the outlet region (Y-Y'), (**b**) the direction of the secondary flow vortices and present forces applying on a particle (according to its location in the cross section) in the microchannel.

Since there exists a secondary flow in the curvilinear microchannel, the particles move in transverse direction (relative to the main fluid flow). To appropriately investigate the particle motion, it is preferred to consider the particles' position in two specific cross sections: transition region and outlet region, as depicted in Figure 1(a). Because of the presence of an inflection point at the transition region and to avoid further confusion, the wall between X and Y is labelled as W_2 and the one between X' and Y' is labelled as W_1.

A parameter that has a major effect on the movement of a microparticle in microchannels is the mean velocity profile. Noteworthy, in straight microchannels, the fluid flow has a 3D parabolic velocity profile, the maximum of which occurs at the center point of the channel cross section and its zero values occur on the walls. Accordingly, at each cross section, SGLF acts on the particles from the center point towards the walls. The magnitude of this force at the centerline is zero. For the case of curved channels, the maximum of the velocity does not occur at the centerline of the microchannel because of the presence of secondary flow (Dean flow) [51]. Dean flow consists of two counter-rotating vortices in transverse direction. At the mid-height of the channel, the secondary flow directs towards the outer wall. In addition, two zero Dean velocity lines exist close to the upper and lower walls of the microchannel. Between each of these lines and their corresponding wall, the secondary flow directs towards the inner wall. Between the two zero Dean velocity lines, its direction is the

Preprints (www.preprints.org) | NOT PEER-REVIEWED | Posted: 2 July 2018 doi:10.20944/preprints201807.0006.v1

other way around. (Figure 1(b)). Additionally, in the microfluidics studies with particle or cell separation scopes and having a spiral geometry, this pattern is preserved up to a specific Dean number [40]. According to some numerical studies, the main flow velocity has a maximum somewhere between the centerline and the inner wall [53,63]. For a particle located between zero Dean velocity lines, the direction of the acting NILF is towards the inner wall. When particles are near the outer wall, the direction of NILF is the same as that of DDF. Thus, particles migrate transversally along the rotational direction of the secondary vortices. Near the centerline, moreover, there is a shift in the velocity profile and, hence, SGLF decreases. Hence, in spiral microchannels the particle stream focuses near the inner wall.

For an alternating curvilinear geometry, any change in the curvature yields in a change in the directions of the secondary flow, and the case becomes more sophisticated compared to spiral microchannels. Therefore, it is a challenging task to accurately anticipate the steady state condition of Dean vortices. It is demonstrated in our previous work that in a symmetric curvilinear microchannel with a uniform width of 350 μm and having a curvature angle of 280°, when the fluid flow is approaching the transition region, a shift in the velocity maxima is observed near the centerline of the channel. Thereafter, the outer wall becomes the inner wall and velocity maxima occurs closer to the inner wall, rather than the centerline. This is in a general agreement with a similar study on asymmetric curvilinear microchannels [52]. Hence, SGLF changes in both horizontal and vertical directions due to these continuous shifts in the velocity maxima in the cross section. The particles focal positions and widths versus Reynolds number are plotted in Figure 2.

This section may be divided by subheadings. It should provide a concise and precise description of the experimental results, their interpretation as well as the experimental conclusions that can be drawn.

3.1. Large particles

At low Reynolds numbers (Re~30) and in the transition region, focusing position of large particles (a= 20 μm, λ_1= 0.139, λ_2= 0.129) is deviated from the centerline slightly towards W_1 spreading over a band which has a width of approximately seven times the diameter of a single particle (Figures. 2(a) and 3(a)). This is because of the insignificant magnitudes of flow velocity and NILF and DDF. As the particles pass along the outlet region, the band is widened by a factor of around 1.5 (Figures. 2(d) and 3(d)) since DDF increases and SGLF decreases. When Re is approximately 53, a particle streak having a width twice a single particle's diameter forms in the transition region. Similar to lower Re, the streak is deviated from the centerline slightly towards W_1. At this Re, the particle focusing behavior in the outlet region is different. Although the focusing width becomes smaller compared to lower Re values, it is still about five times the diameter of a single particle. This wide stream is still closer to the outer wall. It can be claimed that the ratio of NILF to DDF, F_L/F_D , is higher in the transition region because the channel hydraulic diameter D_h is smaller in this region (143 μm versus 152 μm for the outlet region). Similar to the symmetric channel with the same angle of curvature, in the outlet region SGLF acts on the particle towards the outer wall, whilst DDF has an opposite direction. This is due to the assumption of the particles to be between the two zero Dean velocity lines. When the particle stream approaches the transition region, it narrows since F_S increases and F_D decreases. On the other hand, when a particle approaches the outlet region, F_S decreases and F_D increases. Because of the mixing effect of Dean vortices, single particle stream at the transition region widens when reaches the outlet region. However, both F_S and F_D increase with main flow velocity ($F_L \propto U_f^2$, $F_D \propto U_f^{1.63}$). Therefore, at Re~53, large particles focus as a relatively tight stream in both transition and outlet regions. In addition, the lift coefficient decreases with the flow velocity; therefore, DDF exhibits a larger increasing trend compared to the SGLF. Consequently, the particle stream is closer to W_2 in the transition region and moves towards the inner wall in the outlet region. When Re >172, particles stream approaches W_2 in the transition region and, consequently, is repelled by WILF of this wall. At the same time, the particles are pushed away from the velocity maxima towards W_2. It is worth mentioning that as a result of the curvilinear geometry and aforementioned lift and drag forces, the particles do not follow the essential flow

Preprints (www.preprints.org) | NOT PEER-REVIEWED | Posted: 2 July 2018 doi:10.20944/preprints201807.0006.v1

streamlines, rather they migrate perpendicular to them as they approach the outer wall or W_2. Moreover, the focusing width remains unchanged for $53 \leq Re \leq 205$ and $68 \leq Re \leq 189$ in the transition (Figures 2(a) and 2(d)) and outlet regions (Figures 3(a) and 3(d)), respectively.

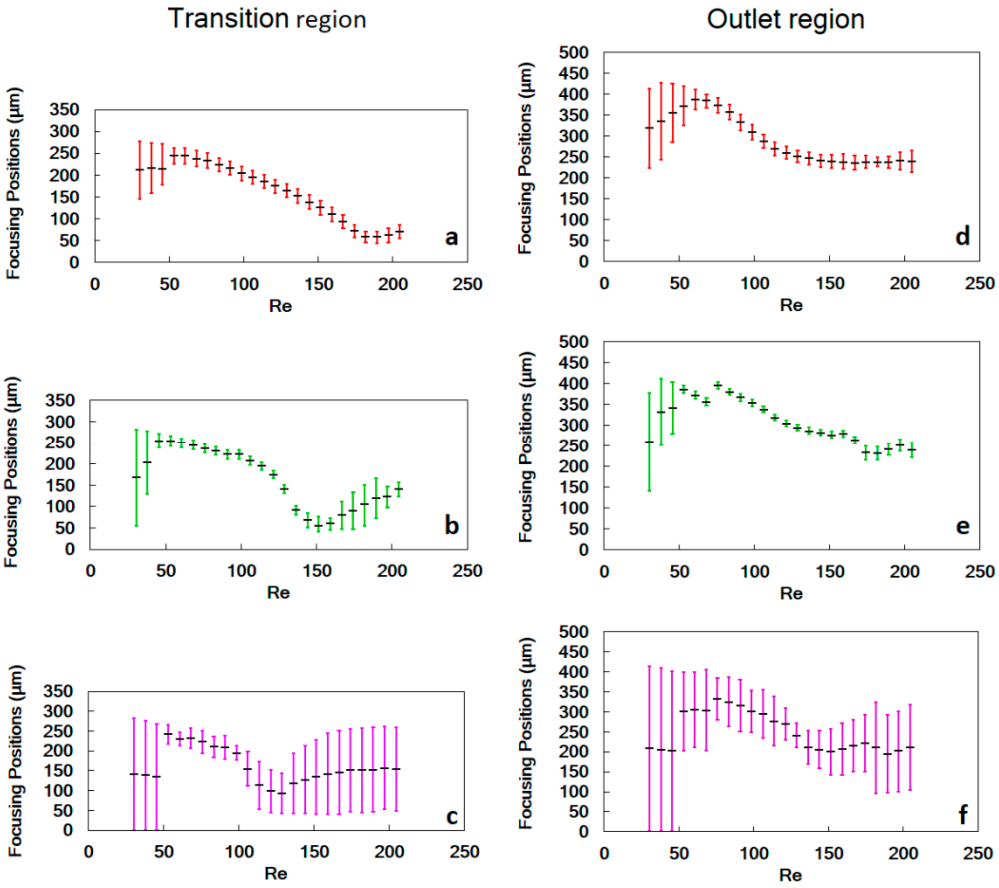

Figure 2. Focusing position against Reynolds number at the transition region for particles of (**a**) 20 μm, (**b**) 15 μm and (**c**) 10 μm diameter and at the outlet region for particles of (**d**) 20 μm, (**e**) 15 μm and (**f**) 10 μm diameter. The width of the focusing bands is shown by error bars. The focal positions of 0 and 350 μm in (**a**-**c**) correspond to walls W_2 and W_1, and 0 and 500 μm in (**d**-**f**) represent inner and outer walls, respectively.

3.2 Medium particles

At low Reynolds numbers (Re~30) and in the outlet region, medium particles (a = 15 μm, λ_1= 0.1, λ_2= 0.09) cover half width of the microchannel at the centerline, while they do not focus at the transition region. The reason is that at low flow velocities, the magnitudes of SGLF and DDF are not high enough to influence the particles. With increasing Re to 45, the particles focus in a band with a width approximately two times a single particle's diameter in the middle of the distance between the centerline and wall W_1 in the transition region (Figures 2(b) and 3(b)). However, such a tight stream is not observed in the outlet region for the same Re (Figures 2(e) and 3(e)). The focusing behavior of medium particles are like that of large particles; as they approach the outlet region, DDF increases and SGLF decreases due to increasing D_h. By increasing Reynolds number, single particle stream gradually moves away from W_1. Because both horizontal and vertical components of SGLF scale with a^3 and DDF with a, medium particles are repelled by the top and bottom channel walls less than large particles at the same flow rate, and they tend to focus near the zero Dean velocity lines. The vertical position of medium particles seems to be between the upper and lower zero Dean velocity lines when they start the transverse motion. In this case, although the direction of SGLF is the same (towards W_2), DDF direction changes from W_2 to the centerline in the transition region. Since there exists a strong reciprocal relationship between the lift coefficient and the main flow velocity [62], as the flow velocity increases, NILF declines in both horizontal and vertical directions. Consequently,

Preprints (www.preprints.org) | NOT PEER-REVIEWED | Posted: 2 July 2018 doi:10.20944/preprints201807.0006.v1

medium particles tend to move to half height of the microchannel, at which the Dean flow directs towards the outer wall. Here, the directions of SGLF and DDF are towards the outer wall in the transition region. Moreover, above Re~144, the particles start to lose their focusing trend in the transition region.

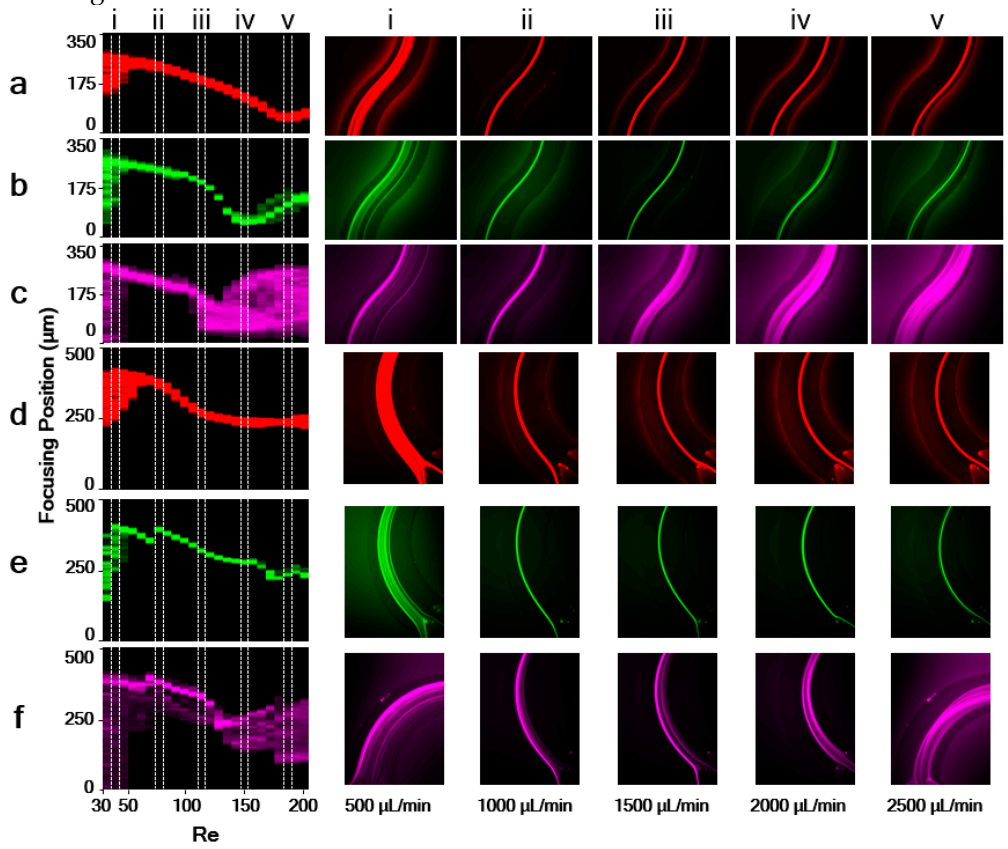

Figure 3. Re maps of the asymmetric curvilinear microchannel in the transition region for micoparticles of (**a**) 20 μm, (**b**) 15 μm, (**c**) 10 μm diameter, and in the outlet region for microparticles of (**d**) 20 μm, (**e**) 15 μm, (**f**) 10 μm diameter. (i–v): Real images of the particles flow at five rates indicated (Main flow direction is downward in all of the images).

3.3 Small particles

For Reynolds numbers below 50, small particles (a = 10 μm, λ_1= 0.069, λ_2= 0.064) focus neither in the transition region (Figures 2(c) and 3(c)) nor in the outlet region (Figures 2(f) and 3(f)). For 53≤ Re ≤106, they tend to focus in the transition region as a very wide band (compared to the diameter of single particles). However, the focusing band migrates through the centerline because F_S, directing towards the inner wall, is a stronger function of the main flow velocity compared to F_D ($F_S \propto U_f^2$, $F_D \propto U_f^{1.63}$), which is in the opposite direction. In the transition region, increasing Re beyond 106 results in a sudden defocusing behavior, which is probably because the vertical position of small particles approaches half height of the channel, at which DDF is reversed in direction. DDF and SGLF have identical directions (towards W_2 in the transition and the outer wall in the outlet region). Therefore, in the transition region, particles approach W_2 with increasing Re to 129. Increasing the flow rate causes a mixing effect on the microparticles because as mentioned before, lift coefficient decreases with the flow velocity, and at some point, SGLF gets smaller than DDF. Furthermore, although the previous studies claimed the lowest limit of particle diameter to channel hydraulic ratio ($\lambda = a/D_h$) be 0.07 for successful particle focusing, the small particles still focus in a relatively wide band (width of four times a single particle diameter) while their λ is about 0.064.

Preprints (www.preprints.org) | NOT PEER-REVIEWED | Posted: 2 July 2018 doi:10.20944/preprints201807.0006.v1

3.4 Discussion

Our experimental observations and results highlight a shift in particle focusing behavior between the transition and outlet regions. Accordingly, it is recommended to carefully locate the outlets at the transition region in alternating curved microchannels, which suggests the potential use of the proposed geometry to separate particles/cells of 10, 15 and 20 μm diameter. Figure 4 illustrates the fluorescent images of particles focusing positions in the asymmetric curved microchannel in the transition region. In the current design, the optimum separation of 20 μm from 15 μm particles occurs at Re~144. The focusing band of the large particles is apart from that of medium ones by a distance of approximately 40 μm, which is about twice the diameter of large particles (Figure 4(a)). As illustrated in Figure 4(b), the enrichment of 20 μm and 10 μm particles is achieved at Re~121 since large particles pass near the centerline while most of small particles travel between the centerline and W_2. Similarly, enrichment of 15 μm and 10 μm particles is achieved at Re~121. According to Figure 4(c), the stream of medium particles is seen near the centerline, while most of small particles travel between the centerline and W_2.

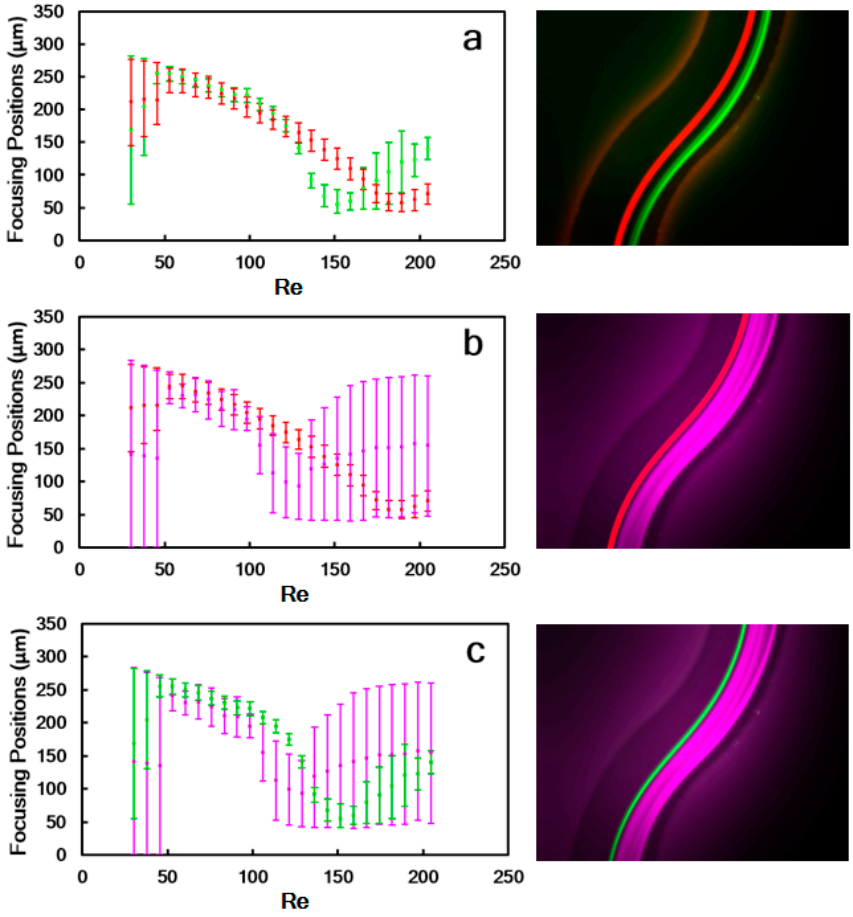

Figure 4. Focusing positions of microparticles at transition region for different flow rates (left column), particle streams for optimum separation or enrichment potential Reynolds number (right column) (**a**) 20 μm and 15 μm, (**b**) 20 μm and 10 μm, (**c**) 15 μm and 10 μm.

Inertial focusing in a symmetric microchannel with the same curvature angle of 280° was previously studied in our group [53]. The focusing behavior of microparticles of the same diameters in an asymmetric microchannel is also compared to that in our previous study. Figure 5 illustrates the focusing position and width of the microparticles in symmetric and asymmetric microchannels. According to Figure 5(a), 20 μm particles focus as narrower bands closer to W_1 for Reynolds numbers between 53 and 106 in the asymmetric microchannel. For Reynolds numbers higher than 136, they focus closer to W_2 in the asymmetric microchannel while their width is almost identical to that in the symmetric microchannel. Figure 5(b) corresponds to 15 μm particles. Accordingly, they tend to focus

Preprints (www.preprints.org) | NOT PEER-REVIEWED | Posted: 2 July 2018 doi:10.20944/preprints201807.0006.v1

closer to W_1 in the asymmetric microchannel for Reynolds numbers up to approximately 114. Beyond this Reynolds number, there is no consistent pattern in the width and position of the particles streams. However, the largest distance between the focusing bands of these particles in the symmetric channel is three times as big as the one in the asymmetric channel. In better words, the symmetric microchannel exhibits a higher separation potential for the current particles sizes. According to Figure 5(c), the width of the focal band is smaller in the asymmetric microchannel over the entire Reynolds number range. Moreover, it is separated from W_2, unlike in the symmetric microchannel, which is in contrast to the previous lower limit of $\lambda/D_h = 0.07$ for successful focusing to occur. Additionally, the focusing width is noticeably smaller in the asymmetric microchannel for Reynolds numbers higher than 53.

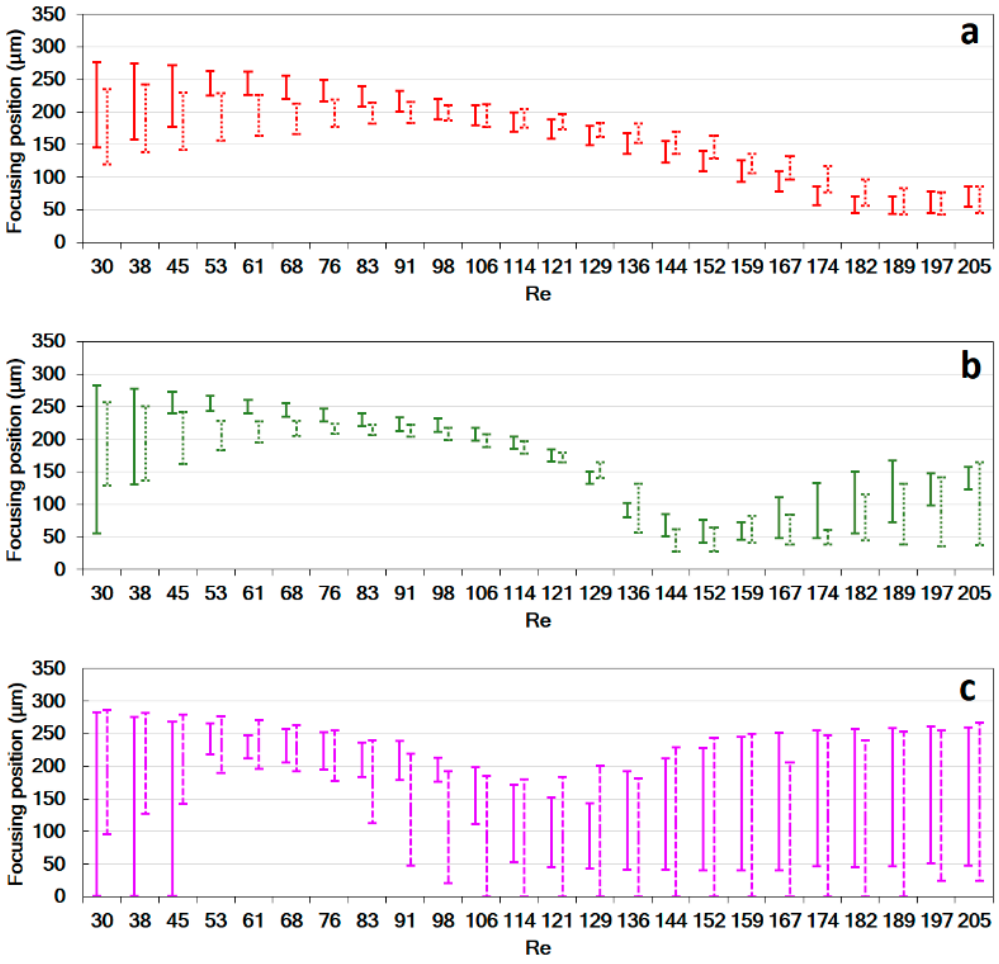

Figure 5. Focusing position against Reynolds number for microparticles of (**a**) 20 μm, (**b**) 15 μm, and (**c**) 10 μm diameter in the transition region of asymmetric (solid bars) and symmetric [53] (dashed bars) curvilinear microchanfgfigfinels, both having curvature angle of 280°.

5. Conclusions

In this study, the focusing behavior of microparticles in an asymmetric curvilinear microchannel was experimentally investigated for particles of 10, 15 and 20 μm diameter, which could be representatives of different cells. Major conclusions are as follows:

- The focusing of large particles occurred in the transition region over a band having width of approximately 1.5 times the diameter of a single particle for Reynolds numbers between 106 and 205, while the focusing width was at least six times larger than that value in the outlet region over the same Re range.
- Medium particles covered a band having a width less than 1.5 times the diameter of a single particle in the transition region for Re of 61-136. They focused in a line having a width of

 doi:10.20944/preprints201807.0006.v1

approximately the diameter of a single particle for Re values between 76 and 167 in the outlet region.

- The minimum width of the focusing band for small particles in the transition region was 3.6 times the diameter of a single particle at Re of 98. This value for the outlet region was at least ten times as big as the diameter of a single particle.
- Focusing behavior of small particles in the proposed asymmetric microchannel significantly differs from the symmetric channel. The dissimilarities include narrower focusing band and noticeable distance from the wall W_2 for the asymmetric microchannel.
- Placing the outlets at the transition region implies the potential use of the proposed geometry in particle or cell separation applications. At Re of 121, the streams of large and small particles were separated by the largest distance, similar to medium and small particles. The separation of large and medium particles was obtained at Re of 144 with a distance of around two times the diameter of large particles.

Author Contributions: Conceptualization, A.K., A.O., and M.K.; Data Curation, A.O. and M.K.; Formal Analysis, A.K., A.O., and M.K.; Funding acquisition, A.K.; Investigation, A.O. and M.K.; Methodology, A.O. and M.K.; Project Administration: A.K., A.O., and M.K.; Supervision, A.K.; Validation, A.K., A.O., and M.K.; Visualization, A.O., M.K., and H.A.; Writing - Original Draft Preparation, A.O.; Writing - Review & Editing, A.K., A.O., M.K., and H.A.

Funding: This work was supported by the Sabanci University Internal Research Grant, No. IACF15-1444, Science Academy Outstanding Young Investigator Support Program (BAGEP), Turkish Academy of Science (TUBA) and Outstanding Young Investigator Support Program (GEBIP).

Acknowledgments: The authors would like to thank Dr. Batu Erman from Molecular Biology, Genetics and Bioengineering Program at Sabanci University for scientifically-rich consultations. The authors utilized the equipment of Sabanci University Nanotechnology Research and Application Center (SUNUM) and Faculty of Engineering and Natural Sciences (FENS) of Sabanci University.

Conflicts of Interest: The authors declare no conflict of interest.

References

1. Oda, R. P.; Strausbauch, M. A.; Huhmer, A. F. R.; Borson, N.; Jurrens, S. R.; Craighead, J.; Wettstein, P. J.; Eckloff, B.; Kline, B.; Landers, J. P. Infrared-mediated thermocycling for ultrafast polymerase chain reaction amplification of DNA. *Anal. Chem.* **1998**, *70*, 4361–4368.
2. Wilding, P.; Shoffner, M. A.; Kricka, L. J. PCR in a silicon microstructure. *Clin. Chem.* **1994**, *40*, 1815–1818.
3. Burns, M. A.; Johnson, B. N.; Brahmasandra, S. N.; Kalyan, H.; James, R. W.; Madhavi, K.; Timothy S.S. An integrated nanoliter DNA analysis device. *Science (80-.).* **1998**, *282*, 484–487.
4. Altendorf, E.; Zebert, D.; Holl, M.; Vannelli, A.; Wu, C.; Schulte, T. Results obtained using a prototype microfluidics-based hematology analyzer. In *Micro Total Analysis Systems*; Springer: Netherlands, 1998; pp. 73–76.
5. Fu, A.; Spence, C.; Scherer, A.; Arnold, F. A microfabricated fluorescence-activated cell sorter. *Nat. Biotechnol.* **1999**, *17*, 1109–1111, doi:10.1038/15095.
6. Knight, J. B.; Vishwanath, A.; Brody, J. P.; Austin, R. H.; Manz, A. Hydrodynamic Focusing on a Silicon Chip: Mixing Nanoliters in Microseconds. *Phys. Rev. Lett.* **1998**, *80*, 3863–3866, doi:10.1103/PhysRevLett.80.3863.
7. Eijkel, J. C. .; Prak, A.; Cowen, S.; Craston, D. H.; Manz, A. Micromachined heated chemical reactor for pre-column derivatisation. *J. Chromatogr. A* **1998**, *815*, 265–271, doi:10.1016/S0021-9673(98)00459-2.
8. Li, D. *Encyclopedia of microfluidics and nanofluidics*; Springer Science & Business Media, 2008;
9. Jacobson, S. C.; Hergenroder, R.; Moore, A. W. J.; Ramsey J.M. Precolumn reactions with electrophoretic analysis integrated on a microchip. *Anal. Chem.* **1994**, *66*, 4127–4132.
10. Tabeling, P. *Introduction to microfluidics*; Oxford University Press.: New York, 2005;
11. Tian, W. C.; Finehout, E. *Microfluidics for biological applications*; 16th ed.; Springer Science & Business Media, 2009;
12. Berthier, J.; Silberzan, P. *Microfluidics for biotechnology*; Artech House, 2010;
13. Nguyen, N. T.; Wereley, S. T. *Fundamentals and applications of microfluidics*; Artech House, 2002;

14. Autebert, J.; Coudert, B.; Bidard, F.; Pierga, J.; Descroix, S.; Malaquin, L.; Viovy, J. Microfluidic: An innovative tool for efficient cell sorting. *Methods* **2012**, *57*, 297–307, doi:10.1016/j.ymeth.2012.07.002.
15. Bhagat, A. A. S.; Bow, H.; Hou, H. W.; Tan, S. J.; Han, J.; Lim, C. T. Microfluidics for cell separation. *Med. Biol. Eng. Comput.* **2010**, *48*, 999–1014, doi:10.1007/s11517-010-0611-4.
16. Arifin, D. R.; Yeo, L. Y.; Friend, J. R. Microfluidic blood plasma separation via bulk electrohydrodynamic flows. *Biomicrofluidics* **2007**, *1*, 14103.
17. Shi, J.; Huang, H.; Stratton, Z.; Huang, Y.; Huang, T. J. Continuous particle separation in a microfluidic channel via standing surface acoustic waves (SSAW). *Lab Chip* **2009**, *9*, 3354–3359, doi:10.1039/b915113c.
18. Hejazian, M.; Li, W.; Nguyen, N.-T. Lab on a chip for continuous-flow magnetic cell separation. *Lab Chip* **2015**, *15*, 959–970, doi:10.1039/C4LC01422G.
19. Jubery, T. Z.; Srivastava, S. K.; Dutta, P. Dielectrophoretic separation of bioparticles in microdevices: A review. *Electrophoresis* **2014**, *35*, 691–713, doi:10.1002/elps.201300424.
20. Mulvana, H.; Cochran, S.; Hill, M. Ultrasound assisted particle and cell manipulation on-chip. *Adv. Drug Deliv. Rev.* **2013**, *65*, 1600–1610, doi:10.1016/j.addr.2013.07.016.
21. Bhagat, A. A. S.; Kuntaegowdanahalli, S. S.; Papautsky, I. Enhanced particle filtration in straight microchannels using shear-modulated inertial migration. *Phys. Fluids* **2008**, *20*, 101702, doi:10.1063/1.2998844.
22. Liu, C.; Hu, G.; Jiang, X.; Sun, J. Inertial focusing of spherical particles in rectangular microchannels over a wide range of Reynolds numbers. *Lab Chip* **2015**, *15*, 1168–1177.
23. Wang, X.; Zandi, M.; Ho, C.-C.; Kaval, N.; Papautsky, I. Single stream inertial focusing in a straight microchannel. *Lab Chip* **2015**, *15*, 1812–1821, doi:10.1039/C4LC01462F.
24. Kim, Y. W.; Yoo, J. Y. The lateral migration of neutrally-buoyant spheres transported through square microchannels. *J. Micromechanics Microengineering* **2008**, *18*, 065015, doi:10.1088/0960-1317/18/6/065015.
25. Chun, B.; Ladd, A. J. C. Inertial migration of neutrally buoyant particles in a square duct: An investigation of multiple equilibrium positions. *Phys. Fluids* **2006**, *18*, 031704, doi:10.1063/1.2176587.
26. Bhagat, A. A. S.; Kuntaegowdanahalli, S. S.; Papautsky, I. Inertial microfluidics for continuous particle filtration and extraction. *Microfluid. Nanofluidics* **2009**, *7*, 217–226, doi:10.1007/s10404-008-0377-2.
27. Zhou, J.; Papautsky, I. Fundamentals of inertial focusing in microchannels. *Lab Chip* **2013**, *13*, 1121, doi:10.1039/c2lc41248a.
28. Hur, S. C.; Brinckerhoff, T. Z.; Walthers, C. M.; Dunn, J. C. Y.; Di Carlo, D. Label-Free Enrichment of Adrenal Cortical Progenitor Cells Using Inertial Microfluidics. *PLoS One* **2012**, *7*, e46550, doi:10.1371/journal.pone.0046550.
29. Mach, A. J.; Di Carlo, D. Continuous scalable blood filtration device using inertial microfluidics. *Biotechnol. Bioeng.* **2010**, *107*, 302–311, doi:10.1002/bit.22833.
30. Zhang, J.; Li, M.; Li, W. H.; Alici, G. Inertial focusing in a straight channel with asymmetrical expansion–contraction cavity arrays using two secondary flows. *J. Micromechanics Microengineering* **2013**, *23*, 85023.
31. Lee, M. G.; Choi, S.; Kim, H.-J.; Lim, H. K.; Kim, J.-H.; Huh, N.; Park, J.-K. Inertial blood plasma separation in a contraction-expansion array microchannel. *Appl. Phys. Lett.* **2011**, *98*, 253702, doi:10.1063/1.3601745.
32. Lee, M. G.; Choi, S.; Park, J.-K. Inertial separation in a contraction–expansion array microchannel. *J. Chromatogr. A* **2011**, *1218*, 4138–4143, doi:10.1016/j.chroma.2010.11.081.
33. Warkiani, M. E.; Tay, A. K. P.; Khoo, B. L.; Xiaofeng, X.; Han, J.; Lim, C. T. Malaria detection using inertial microfluidics. *Lab Chip* **2015**, *15*, 1101–1109, doi:10.1039/C4LC01058B.
34. Bhagat, A. A. S.; Hou, H. W.; Li, L. D.; Lim, C. T.; Han, J. Pinched flow coupled shear-modulated inertial microfluidics for high-throughput rare blood cell separation. *Lab Chip* **2011**, *11*, 1870–1878.
35. Lee, M. G.; Shin, J. H.; Bae, C. Y.; Choi, S.; Park, J.-K. Label-Free Cancer Cell Separation from Human Whole Blood Using Inertial Microfluidics at Low Shear Stress. *Anal. Chem.* **2013**, *85*, 6213–6218, doi:10.1021/ac4006149.
36. Park, J.-S.; Song, S.-H.; Jung, H.-I. Continuous focusing of microparticles using inertial lift force and vorticity via multi-orifice microfluidic channels. *Lab Chip* **2009**, *9*, 939–948, doi:10.1039/B813952K.
37. Bhagat, A. A. S.; Kuntaegowdanahalli, S. S.; Dionysiou, D. D.; Papautsky, I. Spiral microfluidic nanoparticle separators. In *MOEMS-MEMS 2008 Micro and Nanofabrication. International Society for Optics and Photonics.*; 2008; p. 68860M.
38. Martel, J. M.; Toner, M. Inertial focusing dynamics in spiral microchannels. *Phys. Fluids* **2012**, *24*, 032001, doi:10.1063/1.3681228.

39. Guan, G.; Wu, L.; Bhagat, A.; Li, Z.; Chen, P.; Chao, S. Spiral microchannel with rectangular and trapezoidal cross-sections for size based particle separation. *Sci. Rep.* **2013**, *3*, 1475.
40. Bhagat, A. A. S.; Kuntaegowdanahalli, S. S.; Papautsky, I. Continuous particle separation in spiral microchannels using dean flows and differential migration. *Lab Chip* **2008**, *8*, 1906, doi:10.1039/b807107a.
41. Warkiani, M. E.; Guan, G.; Luan, K. B.; Lee, W. C.; Bhagat, A. A. S.; Kant Chaudhuri, P.; Tan, D. S.-W.; Lim, W. T.; Lee, S. C.; Chen, P. C. Y.; Lim, C. T.; Han, J. Slanted spiral microfluidics for the ultra-fast, label-free isolation of circulating tumor cells. *Lab Chip* **2014**, *14*, 128–137, doi:10.1039/C3LC50617G.
42. Warkiani, M. E.; Khoo, B. L.; Tan, D. S.-W.; Bhagat, A. A. S.; Lim, W.-T.; Yap, Y. S.; Lee, S. C.; Soo, R. A.; Han, J.; Lim, C. T. An ultra-high-throughput spiral microfluidic biochip for the enrichment of circulating tumor cells. *Analyst* **2014**, *139*, 3245, doi:10.1039/c4an00355a.
43. Kuntaegowdanahalli, S. S.; Bhagat, A. A. S.; Kumar, G.; Papautsky, I. Inertial microfluidics for continuous particle separation in spiral microchannels. *Lab Chip* **2009**, *9*, 2973, doi:10.1039/b908271a.
44. Bhagat, A. A. S.; Kuntaegowdanahalli, S. S.; Kaval, N.; Seliskar, C. J.; Papautsky, I. Inertial microfluidics for sheath-less high-throughput flow cytometry. *Biomed. Microdevices* **2010**, *12*, 187–195, doi:10.1007/s10544-009-9374-9.
45. Zhang, J.; Yan, S.; Li, W.; Alici, G.; Nguyen, N.-T. High throughput extraction of plasma using a secondary flow-aided inertial microfluidic device. *RSC Adv.* **2014**, *4*, 33149–33159.
46. Li, W.; Yan, S.; Sluyter, R.; Nguyen, N. Inertial particle separation by differential equilibrium positions in a symmetrical serpentine micro-channel. *Sci. Rep.* **2014**, *4*, 4527.
47. Zhang, J.; Li, W.; Li, M.; Alici, G.; Nguyen, N.-T. Particle inertial focusing and its mechanism in a serpentine microchannel. *Microfluid. Nanofluidics* **2014**, *17*, 305–316.
48. Zhu, J.; Canter, R. C.; Keten, G.; Vedantam, P.; Tzeng, T.-R. J.; Xuan, X. Continuous-flow particle and cell separations in a serpentine microchannel via curvature-induced dielectrophoresis. *Microfluid. Nanofluidics* **2011**, *11*, 743–752.
49. Amini, H.; Lee, W.; Di Carlo, D. Inertial microfluidic physics. *Lab Chip* **2014**, *14*, 2739, doi:10.1039/c4lc00128a.
50. Zhang, J.; Yan, S.; Yuan, D.; Alici, G.; Nguyen, N.-T.; Ebrahimi Warkiani, M.; Li, W. Fundamentals and Applications of Inertial Microfluidics: A Review. *Lab Chip* **2016**, *16*, 10–34, doi:10.1039/C5LC01159K.
51. Di Carlo, D. Inertial microfluidics. *Lab Chip* **2009**, *9*, 3038–3046, doi:10.1039/b912547g.
52. Di Carlo, D.; Irimia, D.; Tompkins, R. G.; Toner, M. Continuous inertial focusing, ordering, and separation of particles in microchannels. *Proc. Natl. Acad. Sci. U. S. A.* **2007**, *104*, 18892–18899, doi:10.1073/pnas.0704958104.
53. Özbey, A.; Karimzadehkhouei, M.; Akgönül, S.; Gozuacik, D.; Koşar, A. Inertial Focusing of Microparticles in Curvilinear Microchannels. *Sci. Rep.* **2016**, *6*, 38809.
54. Dino Di Carlo; Jon F. Edd; Daniel Irimia; Ronald G. Tompkins, A.; Toner*, M. Equilibrium Separation and Filtration of Particles Using Differential Inertial Focusing. *Anal. Chem.* **2008**, *80*, 2204–2211, doi:10.1021/AC702283M.
55. Gossett, D. R.; Carlo, D. Di Particle Focusing Mechanisms in Curving Confined Flows. *Anal. Chem.* **2009**, *81*, 8459–8465, doi:10.1021/ac901306y.
56. Vasseur, P.; Cox, R. G.; Feng, J.; Joseph, D. D. The lateral migration of spherical particles sedimenting in a stagnant bounded fluid. *J. Fluid Mech.* **1977**, *80*, 561, doi:10.1017/S0022112077001840.
57. Matas, J.; Morris, J.; Guazzelli, E. Lateral Forces on a Sphere. *Oil Gas Sci. Technol.* **2004**, *59*, 59–70, doi:10.2516/ogst:2004006.
58. Martel, J. M.; Toner, M. Inertial Focusing in Microfluidics. *Annu. Rev. Biomed. Eng.* **2014**, *16*, 371–396, doi:10.1146/annurev-bioeng-121813-120704.
59. Di Carlo, D.; Edd, J. F.; Humphry, K. J.; Stone, H. A.; Toner, M. Particle Segregation and Dynamics in Confined Flows. *Phys. Rev. Lett.* **2009**, *102*, 094503, doi:10.1103/PhysRevLett.102.094503.
60. Zeng, L.; Balachandar, S. Wall-induced forces on a rigid sphere at finite Reynolds number. *J. Fluid Mech.* **2005**, *536*, 1–25.
61. Takemura, F.; Magnaudet, J. The transverse force on clean and contaminated bubbles rising near a vertical wall at moderate Reynolds number. *J. Fluid Mech.* **2003**, *495*, 235–253.
62. Asmolov, E. The inertial lift on a spherical particle in a plane Poiseuille flow at large channel Reynolds number. *J. Fluid Mech.* **1999**, *381*, 63–87.
63. Martel, J.; Toner, M. Particle focusing in curved microfluidic channels. *Sci. Rep.* **2013**, *3*, 3340.